DOE/NV/03624--0819

Drone Video Platform—Collision Avoidance, Situational Awareness, and Communications

STL-039-17 ■ Year 3 of 3

Rusty Trainham,[1,a] Paul Guss,[b] Manuel Manard,[a] Tom Keenan,[a] Edward Bravo,[b] Willy Kaye,[c] and Kevin Kochersberger[d]

[1]trainhcp@nv.doe.gov, (805) 681-2248
[a]Special Technologies Laboratory
[b]Remote Sensing Laboratory–Nellis
[c]H3D Corporation
[d]Virginia Polytechnic Institute and State University

Small unmanned aerial systems are ideal for delivering sensors into areas that are inaccessible or too dangerous for human entry or manned aircraft over-flights. The systems can fly low and slow for enhanced sensitivity and in tight spaces where ordinary aircraft could never fit. We have configured and flown sensor payloads for radiation, chemical, and optical detection on small fixed-wing and rotary-wing aircraft. All the sensor packages provide telemetry, GPS coordinates, LIDAR distance ranging, and absolute time of day to microsecond accuracy. Payload weights range from less than 1 kg up to 5.5 kg. Currently, communications are over 2.4 GHz and 915 MHz radios, as well as over 4G LTE cellular data links. Real-time data feeds from the sensor payloads to web browser clients anywhere in the world are possible via a virtual EC2 server on the Amazon AWS cloud. In FY 2019, the Nevada National Security Site teamed with Virginia Tech, H3D Corp., and Unmanned Systems, Inc. to accomplish the four flight missions described in this report. A large part of this year's mission goals were to demonstrate the ability to fly beyond visual line of sight (BVLOS).

Background

The SDRD small unmanned aerial systems (sUAS) initiative has been exploring niche areas for complementing and expanding Aerial Measuring System (AMS) missions. The Fukushima disaster of 2011 was the wake-up call that made it obvious that AMS platforms simply could not make certain critical measurements over the reactor containment building because of extreme radiation and chemical explosion hazards. In the decade since Fukushima, the SDRD program has been exploring detectors,

platforms, and techniques for aerial measurements of radiation, chemical, and optical characteristics over hazardous environments. Radiation survey flights have been conducted in a variety of locations, such as the Nevada National Security Site (NNSS), Idaho National Laboratory (INL), and Savannah River National Laboratory (SRNL). Chemical plume and optical spectra detection tests were conducted in Montana and Wisconsin. Also, test flights to demonstrate beyond visual line of sight (BVLOS) operations occurred with both fixed-wing aircraft and rotary hexacopters at Camp Roberts, California.

For safety reasons, manned aircraft typically fly radiation surveys at altitudes of 350 meters above ground level (AGL) and higher and at fairly high speeds. Small UASs, on the other hand, can fly at a few meters AGL and significantly slower than manned aircraft, a distinct advantage for radiation detection missions. The much lower altitude also results in radiation maps with greater geographical detail. Because UASs can withstand higher radiation doses without operational issues, a heavily contaminated one can be "sacrificed."

In spite of their advantages, UASs do have two significant limitations: lower weight payload capacity and shorter flight times. In principle, larger unmanned aircraft (e.g., Predator, Reaper, or Global Hawk) can be equipped to carry the same NATO radiation detection pod as an AMS aircraft for as long as necessary to complete a typical AMS survey. However, there is not much community appeal in using such large assets to fly AMS missions; therefore, there is greater interest in using small COTS aircraft to conduct narrowly targeted radiation surveys using smaller detector payloads on briefer flights.

Project

Our previous report (Trainham 2019) described the detectors, platforms, and capabilities that we have developed during the SDRD UAS initiative; in the current report we discuss four missions undertaken since then. Over the past year most of our work has been focused on conducting fully autonomous BVLOS flights with an emphasis on radiation detection. The techniques developed are equally applicable to chemical and optical detection, but we chose to fly the radiation detectors because those particular missions are easier to coordinate. The first mission at the Desert Rock Airstrip (DRA) was a catastrophic failure resulting in total loss of a Sandstorm fixed-wing drone. The other missions—one at SRNL and two at Camp Roberts, California—were mostly successful. Complete success has been elusive thus far, primarily because of persistent radio communications problems between the ground station and the aircraft.

Desert Rock Airstrip Crash

On November 9, 2018 at 1:59 p.m., the Sandstorm N778VF crashed about 0.5 miles west of the Desert Rock Airport after 19 minutes of flight time. Figure 1 shows the flight path prior to the crash from GPS data recovered from the detector pod. This dry run flight was configured to follow a lawn mower–style radiation survey plan in preparation for an eventual flight over the Baneberry crater at the NNSS. The Sandstorm was carrying a 10-pound detector pod containing a 3×6 sodium iodide (NaI) gamma detector and 21 pounds of Jet Fuel A in the fuel tanks. After recovery, we measured that approximately 6.6 pounds of fuel had been burned during the flight. Inspection of the fuel filter and fuel lines indicated that they were clean and unobstructed. The battery voltages were all within normal range, and there was no indication of a fuel line rupture or electrical failure. The Piccolo autopilot

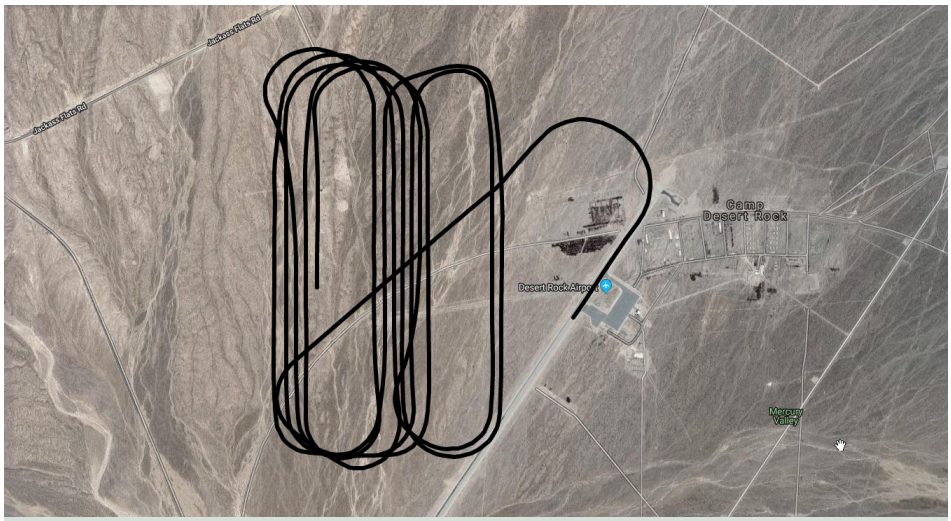

Figure 1. The Sandstorm had flown approximately half of the grid pattern when it suddenly lost power and crashed. This GPS track was recovered from the detector pod's Raspberry Pi.

Figure 2. The Sandstorm crash occurred about 0.5 miles west of the DRA runway

Figure 3. The Sandstorm was banking into a turn when it lost power. Marks in the terrain show the wing and fuselage impact.

and JetCat turbine appeared virtually unscathed by the crash. The Sandstorm air frame, however, was damaged beyond repair, as was the detector pod. The detector inside of the pod was visibly damaged, but still operational. Figures 2 and 3 show the wreckage and impact site, respectively.

A GoPro camera had been mounted under the nose of the Sandstorm, and it recorded video throughout the flight. The camera survived the crash and continued recording until it was recovered and switched off. The audio of the video provides a clear recording of the sound of the turbine during the flight. What appears to be significant is that the turbine was accelerating and decelerating every few seconds throughout the entire flight. The shutdown of the turbine is clearly audible about 10 seconds before the crash. Several people who have reviewed the video claim that it sounds like a turbine flame out.

Log files from the Piccolo ground station were sent to the manufacturer, Cloud Cap, for review, and Steven Kelley of Cloud Cap confirmed that the autopilot did not command a turbine shutdown. The Piccolo autopilot did issue several terrain warnings when it determined that the altitude had fallen below 200 feet AGL, but the only errors signaled by the Piccolo were drops below minimum set points for altitude and airspeed as the aircraft glided downward after power loss. During the down glide, the Piccolo did attempt to command the turbine to full throttle when it detected loss of airspeed and altitude, but it seemed to be unaware of the turbine power loss. We sent the Piccolo Nano circuit card to Cloud Cap for inspection, and it was found to be fully operational. Steven Kelley of Cloud Cap, however, did strongly advise against installing it in the other Sandstorm, citing possible circuit board stresses that could cause a future failure.

The JetCat SPT5 turbine was shipped to Dreamworks in Virginia for inspection, and it was also found to be fully functional. George DelMoral of Dreamworks read out the data log from the engine control unit (ECU) and confirmed that the turbine had shut down unexpectedly. There was no evidence of fuel pump malfunction, fuel line obstruction, or electrical power loss. His supposition was that an air bubble in the

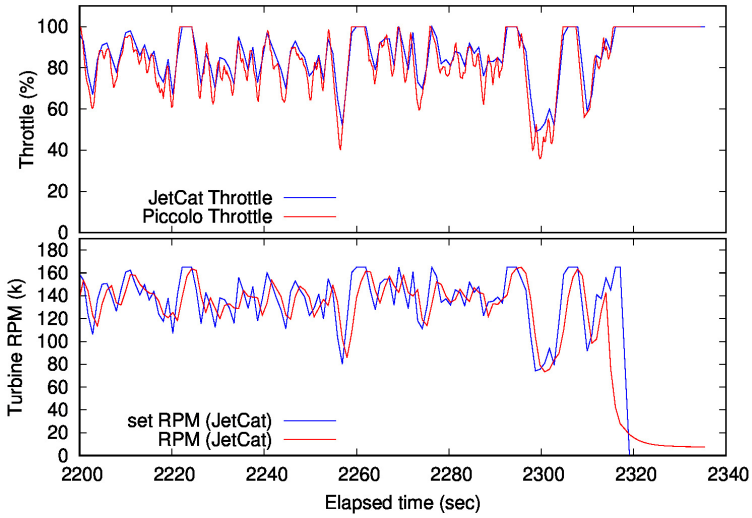

Figure 4. The alignment of the clock signals of the Piccolo and JetCat was done by eye. A 2% change in clock rate and an offset were necessary to synchronize the log files. The zero time is the Piccolo startup.

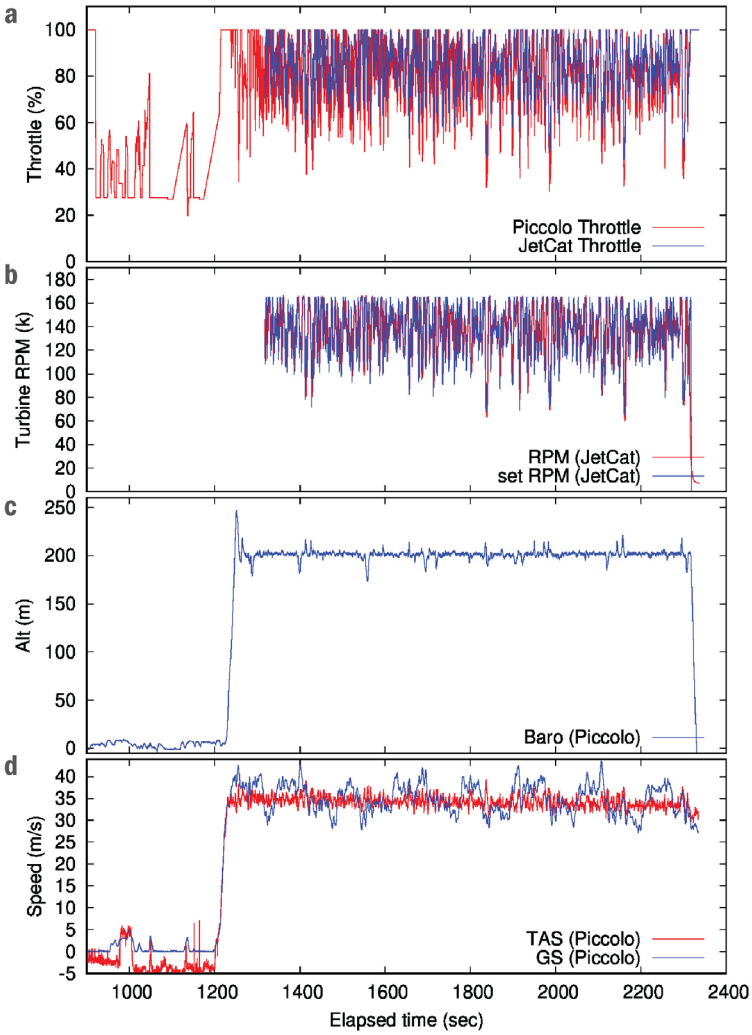

Figure 5. Data from the entire flight are shown here. The JetCat log holds only 1000 seconds of data, so we see only the last 1000 seconds of JetCat data for the flight. The speed and altitude plots are for context, and the compelling data shown here are the throttle and turbine RPM signals.

fuel line caused a flame out. Unfortunately, once the turbine shuts down it cannot be restarted in the air.

The Piccolo and the JetCat do not share a common clock, and their log files contain relative time stamps for elapsed time since system startup. Because they start independently when the batteries are connected, there is no standard means for synchronizing them. For generating the data plots in Figures 4, 5, and 6, we achieved synchronization by aligning the throttle signals at the end of the flight. Figure 4 shows the alignment of the Piccolo and JetCat clock signals during the last two minutes of flight, with not only a time offset, but also a clock rate adjustment of 2%. This procedure was done by eye. The x-axis shows time elapsed from startup of the Piccolo. Figure 5 shows data from the Piccolo and the JetCat for the entire flight: Figure 5a is the throttle signal percentages read from both the Piccolo and the JetCat, Figure 5b is the turbine rotation rate in kRPM read from the JetCat; Figure 5c is the altitude read from the Piccolo; and Figure 5d is the air speed and ground speed read from the Piccolo. Figure 6 shows the throttle and turbine rotation signals along with fuel pump voltage and turbine exhaust temperature over the final 2 minutes of the flight.

Figure 5 also shows that the average throttle setting was nearly 90% throughout the flight, with frequent slews up to full throttle and down to as low as 30% throttle. This should not be considered normal. Having reached cruising altitude, a typical flight's average throttle setting would be about 60%, and only minor adjustments at the 5% level would be appropriate. The behavior seen here suggests that the throttle servo parameters entered into the Piccolo were not properly adjusted for that particular air frame and turbine. The gain was too high and the time constant too short. It is unclear if this mismanagement of the turbine by the Piccolo autopilot could be the cause of a turbine flame out, but the problem needs to be corrected if we intend to use a Piccolo autopilot in the other Sandstorm.

We also observe in Figure 5 that the turbine frequently went to the maximum rotation of 165,000 RPM, and it was frequently allowed to spin down to as low as 60,000 RPM. Those two extremes should be avoided. The speed of the aircraft was at the maximum specified airspeed of 70 mph (35 m/s), which explains the high average throttle setting. Before the flight, we had requested the slowest airspeed possible, which would be consistent with safe flight of the Sandstorm. Why such a high airspeed was programmed into the Piccolo is unknown. While an NNSS employee laid out the basic geographical flight pattern for the autopilot, a contractor to Unmanned Systems, Inc. (USI) conducted the final flight plan verification. This individual was on the original design team of the Piccolo autopilot, and he is considered an expert in Piccolo configuration and operation.

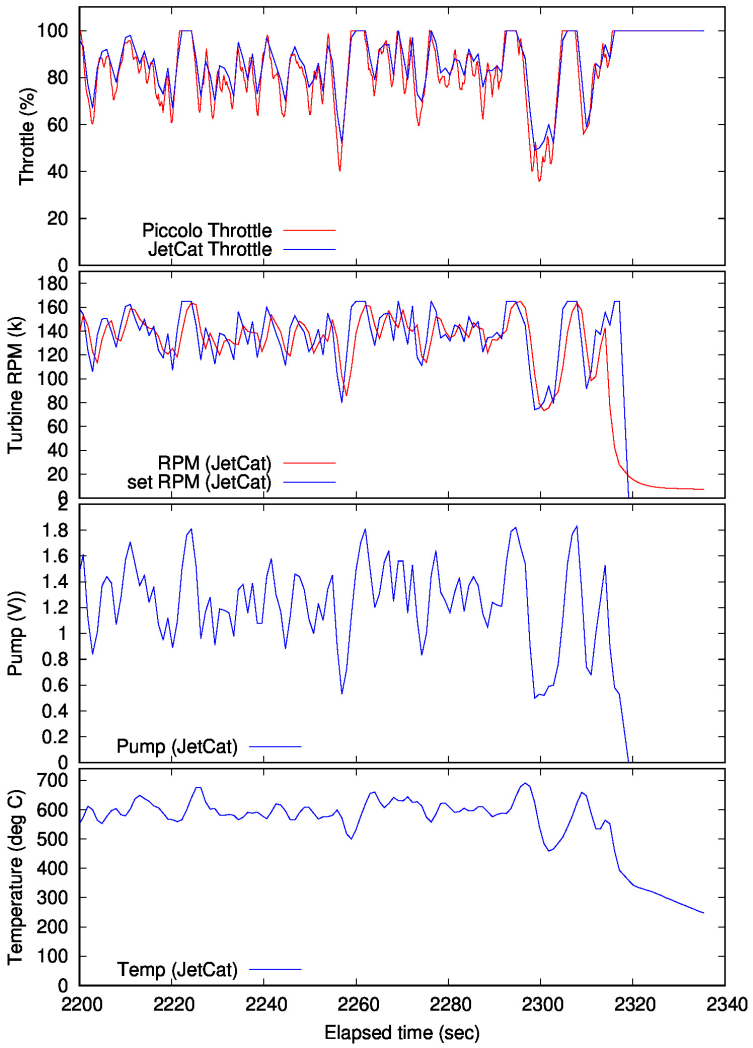

Figure 6. The final 2 minutes of the flight are shown here. At the moment of power failure, the JetCat was being commanded to full throttle.

One further notes a curious feature in Figure 6—the turbine shutdown occurred while the turbine was ramping up again. This occurrence is at odds with the audio of the GoPro video. The audio suggests that the turbine lost power as it was slewing downward. However, the turbine RPM and temperature graphs in Figure 6 clearly indicate that the turbine was ramping up again when it shut down. The audio is rather noisy, though, so observations drawn from it can only delineate coarse features.

In summary, the cause of the crash has not been fully established. The most likely explanation is that an air bubble in the fuel line interrupted fuel flow to the turbine, which then flamed out. The fact that the Piccolo autopilot had not been properly tuned to the time constants of the JetCat turbine can explain the erratic oscillation of the turbine speed, but this information is insufficient to explain a flame out while the turbine was actually accelerating up to full throttle. Although neither the JetCat nor the Piccolo can be held responsible for the crash, the experience has underlined a general dissatisfaction with a turbine that loses power unexpectedly and cannot be restarted in the air, and also a dissatisfaction with the limitations of the Piccolo autopilot, which sensed the imminent crash yet did not deviate from its flight plan.

Hyperion Horntail

During the week of April 22, 2019, a team from the Unmanned Systems Laboratory of Virginia Tech (Va Tech) and NNSS's Special Technologies Laboratory (STL) participated in the Defense Threat Reduction Agency (DTRA)–sponsored Hyperion Horntail exercise at the R Reactor site at SRNL. The event was organized to demonstrate aerial mapping and ground collection of nuclear materials for forensic purposes. The source targets were fifteen radioactive sources placed within a 50-meter-diameter circular pattern on the ground. For the exercise, Va Tech supplied a heavy-lift hexacopter, and STL provided two types of radiation detectors for aerial mapping and gamma imaging, but only the 2×2 NaI was flown to perform aerial radiation mapping. The more sophisticated, yet much heavier, Apollo gamma imaging detector was not flown due to unexpected flight instabilities of the aircraft. These problems had not been previously experienced when lifting the heavier payload. Once the aircraft was back at Va Tech the problem was traced to a defective accelerometer in the autopilot. Nevertheless, seven radiation surveys were flown with the 2×2 NaI detector, and the resulting radiation heat maps are presented in this report.

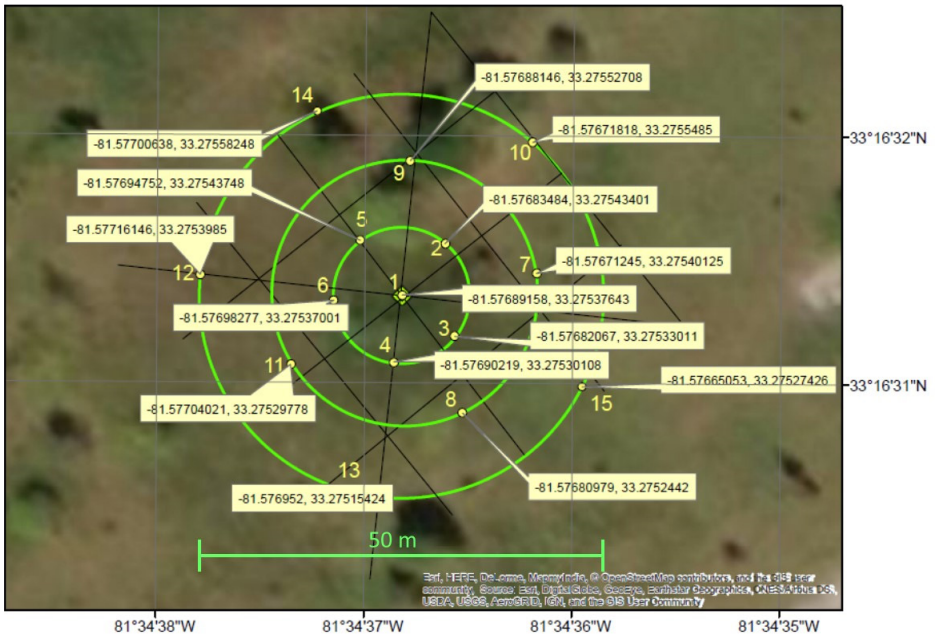

Figure 7. GPS locations of radioactive sources

Aerial debris field mapping (ADFM) is a collaborative research and development effort between Va Tech's Unmanned Systems Lab and the NNSS to assess the use of drones to supplement the AMS mission of the National Nuclear Security Administration (NNSA). The AMS has teams based out of the Remote Sensing Laboratories (RSL) at Nellis Air Force Base in Las Vegas and at the Joint Base Andrews in Washington, D.C. The mission of the AMS is to provide rapid aerial surveys of ground radiation and contamination following a radiological emergency. An AMS deployment for an emergency mobilizes fixed-wing manned aircraft carrying radiation detectors to localize ground contamination, followed by manned helicopter deployment for detailed radiation surveys. In extreme situations, such as experienced at Fukushima, the helicopter surveys present considerable safety risks for personnel on board; therefore, as an alternative to AMS, drone technology could play a decisive role in collecting detailed and actionable data for mapping potential radiation exposure on the ground.

This research was initiated in 2011 through a DTRA basic research grant with the University of Maryland, RSL, and Va Tech. Though not part of the initial research effort, the NNSS Special Technologies Laboratory (STL) has developed sensors for drones under SDRD projects, and in winter 2018, RSL invited STL to provide a radiation detector for the Va Tech hexacopter flight at the Huckleberry Hustle exercise in Idaho. With a CRADA already in place with H3D Corporation of Ann Arbor, Michigan, STL was able to provide H3D's Apollo gamma imaging detector. This detector, which contains four CZT crystals, constructs gamma images by Compton back-projection. At Huckleberry Hustle the results from both the Apollo detector and the 2×2 NaI detector were so compelling that STL, RSL, and Va Tech decided to continue their expanded collaboration. The team also flew tests in Idaho (July 2018) and at the NNSS (late September 2018). When DTRA announced the 2019 Hyperion Horntail exercise, all three organizations requested to participate.

During the DTRA-sponsored Hyperion Horntail exercise at the SRNL, Va Tech, and the NNSS tested radiation survey techniques with a 2×2 NaI detector flown on a hexacopter. While the Apollo detector was present at Hyperion Horntail, its weight caused flight

instabilities that were worrisome. After two days of unsuccessfully troubleshooting, the Apollo flights were scrubbed and the surveys were conducted with the 2×2 NaI detector alone.

Previously, the Huckleberry Hustle exercise provided a venue to detect an explosively dispersed continuous distribution of ^{82}Br radioactive contamination. For the 2019 Hyperion Horntail, by contrast, fifteen discrete milliCurie-level check sources were placed in a 50-meter-diameter circular pattern. The datasets collected in these two exercises would provide a valuable opportunity for comparison and also allow us to test the Laplacian Eigenmapping algorithm's ability to distinguish between continuous and discrete source distributions by the NaI detector. The technique is described by Belkin and Niyogi (2003), and previous results for this application are presented in Peterson et al. (2019).

The distribution pattern and GPS locations of the sources at Hyperion Horntail are shown in Figure 7, and their identities and activities are listed in Table 1. Most of the sources were ^{137}Cs, but the strongest sources at the center of the pattern were ^{60}Co. In addition, ^{152}Eu and ^{133}Ba sources were located in the western half of the circle.

The distance between sources 1 and 2 (both ^{60}Co) was approximately 8.3 meters, and their close proximity on the ground would present a challenge for any technique to resolve separate sources from data collected by an omni-directional detector flying 15 meters overhead. Poisson counting fluctuations would very likely mask the undulations in the data stream from passing over discrete sources so close together.

Table 2 lists the objectives, metrics, and methods from the Hyperion Horntail test execution plan. Some objectives were not achieved due to the circumstance that, as mentioned, the hexacopter experienced flight instabilities when the 10-pound Apollo detector pod was on board. This came as a surprise, since the aircraft had no issues flying the same payload at Huckleberry Hustle the preceding year. We note, however, that the aircraft at Hyperion Horntail was not the heavy-lift hexacopter flown at Huckleberry Hustle, which was destroyed in a crash in July 2018, but it was a hexacopter of identical specifications. Two days of troubleshooting at Hyperion Horntail did not resolve the problem, so the intended Apollo flights were replaced by solo 2×2 NaI flights. Further troubleshooting at Va Tech after the exercise localized the problem to an erratic accelerometer in the Pixhawk autopilot. Because of the flight instability, objective 1

Table 1. Sealed source descriptions

#	ISOTOPE	SERIAL #	ACTIVITY (MCI)	DOSE RATE AT 10 FT (MREM)	DOSE RATE AT 50 FT (MREM)
1	^{60}Co	A-419	9.2	1272	49
2	^{60}Co	I7-788	2.7	373	14
3	^{60}Co	CZ 4948	2.6	360	14
4	^{137}Cs	OF 481	7.5	257	10
5	^{152}Eu	K9-750	3.9	217	
6	^{137}Cs	CZ 2696	4.5	154	6
7	^{60}Co	OM 683	1	138	5
8	^{137}Cs	L-943	2.9	100	4
9	^{137}Cs	L305	2.6	89	3
10	^{137}Cs	L303	2.5	85	3
11	^{137}Cs	L306	2.5	85	3
12	^{133}Ba	K9-884	3.6	76	3
13	^{137}Cs	5152GR	2.2	75	3
14	^{137}Cs	L-627	2	69	3
15	^{137}Cs	K2-132	1.4	48	2

was not fully realized, and objective 4 was not attempted. Objectives 2 and 3, however, were achieved.

The Va Tech–STL team arrived in two vans with equipment for flight operations on Monday, April 22, 2019, and set up by the USMA team next to the HOG 2 area shown in Figure 8. The Va Tech and USMA logos in the figure mark the approximate locations for both groups, but the actual locations of the teams were swapped during the exercise. The marker designated SLA (source layout area) in the figure marks where the radioactive sources were placed.

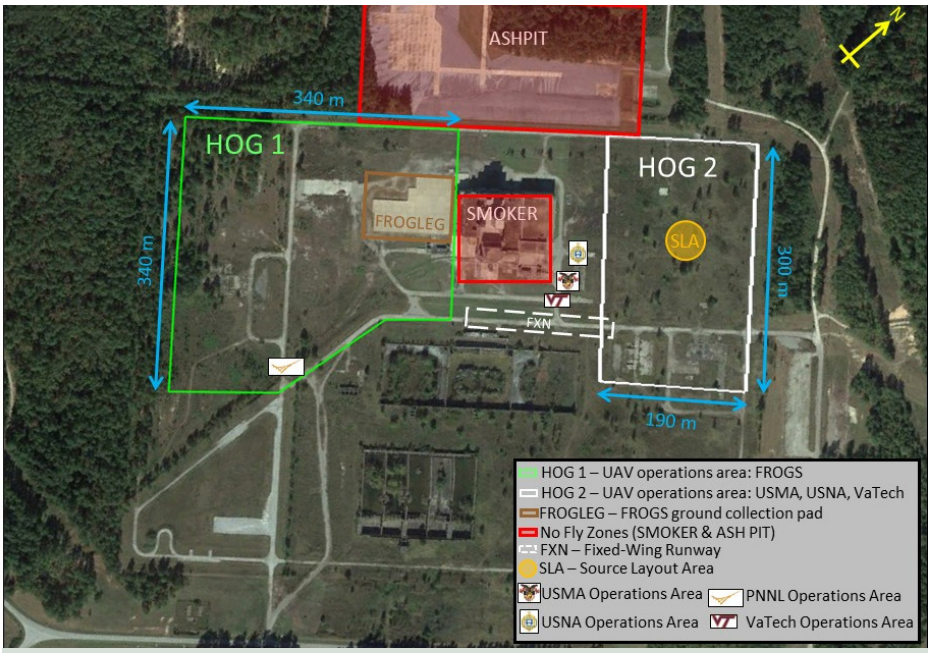

Figure 8. R Reactor Site at SRNL for Hyperion Horntail exercise

Figure 9 shows the Va Tech hexacopter as outfitted for Huckleberry Hustler in 2018, when it carried both the Apollo pod and the 2×2 NaI detector. The NaI detector is mounted on the landing struts beneath the pod.

Details of the Apollo pod's interior are shown in Figure 10. A close-up of the pod mounted on the hexacopter is shown in Figure 11, and the figure also shows the Lightware SF11/C LIDAR and the 2.4 GHz Ubiquiti radio link. Figure 12 shows a close-up of the pod with the nose cone removed. A Raspberry Pi 3B

Table 2. Aerial debris field mapping (ADFM) objectives, metrics, and methods

NATIONAL NUCLEAR SECURITY SITE (NNSS) – AERIAL DEBRIS FIELD MAPPING				
OBJECTIVE	**MEASURE OF PERFORMANCE**	**SUCCESS CRITERIA**	**EVALUATION CRITERIA**	**EXPECTED RESULTS/ FINAL PRODUCT**
1. Ensure the aircraft is operational	1. Equipment operation	1. No failures	1. Assessment of air and ground systems	1. System is fully functional and operationally correct
2. Ensure the payloads are operational	2. Equipment operation	2. No failures	2. Assessment of air and ground systems	2. System is fully functional and operationally correct
3. Collect radiation scan data from NaI sensor	3. Radiation data are above background	3. Radiation data are statistically relevant	3. Statistical analysis	3. Classified source map
4. Collect image data using CZT imager	4. Accuracy of radiation plots	4. Plotted radiation data are shown within an acceptable uncertainty range	4. Correlation of measured with known radiation field	4. Radiation images of area

Methodology: Va Tech will fly multiple survey flights. Some flights will be flown with the NaI and CZT detectors, while other flights will be flown with just the CZT.

Figure 9. Va Tech hexacopter carrying the Apollo gamma imager pod and the 2×2 NaI detector mounted beneath the pod

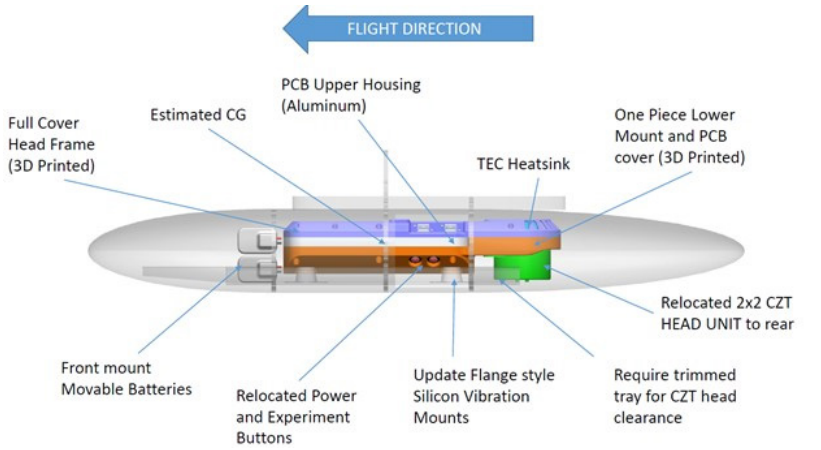

Figure 10. Contents of the pod containing the Apollo gamma imager

communications bridge for the Apollo detector, which was tethered to the Raspberry Pi over a USB serial link; it communicated via TCP/IP packets. In previous exercises the Raspberry Pi communicated to the ground station over a 1 W, 915 MHz, RFD900x radio, however for Hyperion Horntail the Raspberry Pi was linked to the aircraft's Ethernet interface and it communicated to the ground station over the Ubiquiti 2.4 GHz extended Wi-Fi link.

Once GPS lock and communications links had been verified, the Apollo detector itself was turned on. Both the Apollo and the 2×2 NaI detectors were calibrated with a small LYSO crystal containing a few nanoCuries of ^{176}Lu (this isotope has gammas at 202 keV and 306 keV). After the calibrations were completed, background spectra were collected. At this point, communications between the pod and the ground station went through an Apache http server running on the Raspberry Pi.

These pod preparations were typically done before mounting the pod onto the aircraft.

Concurrent with the pod preparations, the pilot-in-charge installed fresh

Figure 11. Close-up pf the Apollo pod and the 2x2 NaI detector mounted beneath the hexacopter with the LIDAR at the top, and the 2.4 GHz Ubiquiti radio mounted on the landing strut in the right foreground.

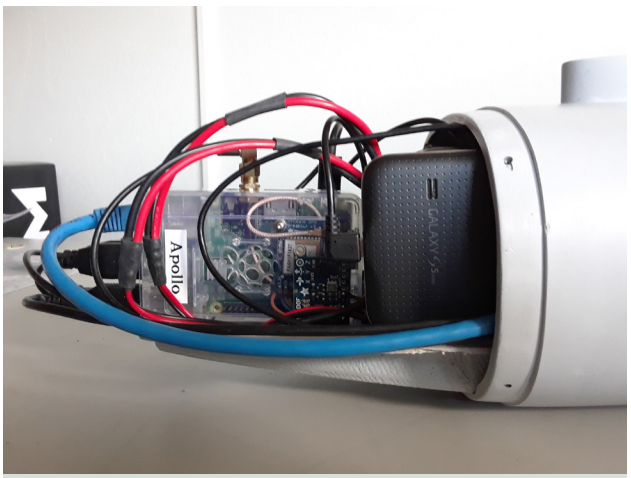

Figure 12. Inside the nose cone of the Apollo pod are the Raspberry Pi 3B computer with GPS receiver and 10DOF telemetry chip. The cell phone for the 4G LTE communications link was not installed for Hyperion Horntail.

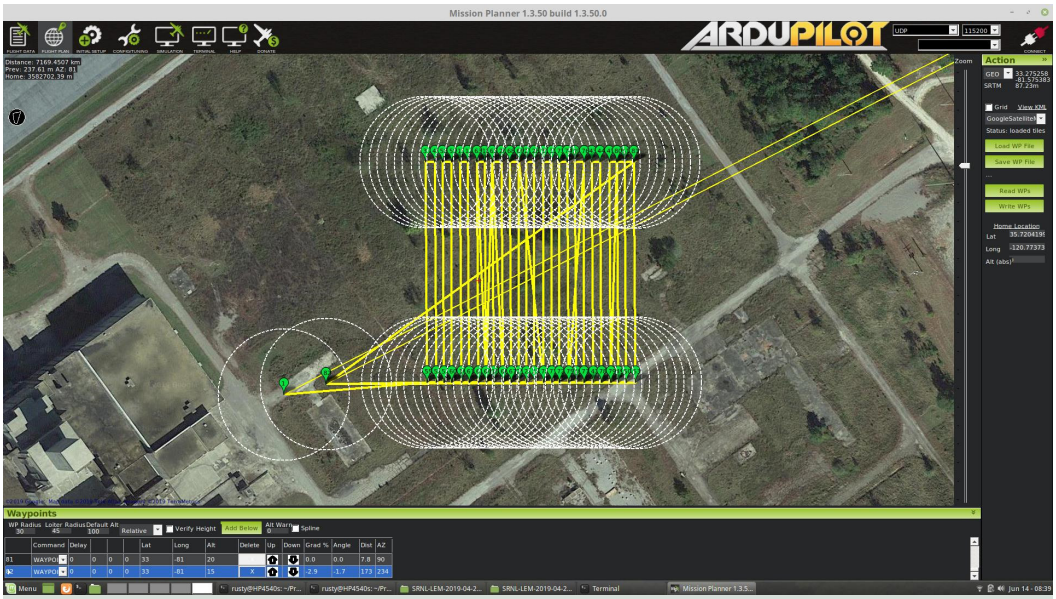

Figure 13. The flight plan for Hyperion Horntail as rendered by the Mission Planner application

batteries on the aircraft, inspected it, and prepared it for flight. The ground control station operator prepared the flight plan in Mission Planner (see Figure 13) and uploaded it to the Pixhawk 2 autopilot.

Preliminary flights were flown with a 10-pound dummy weight in place of the pod to confirm safe flight operations. It was during these preliminary flights that instability issues occurred. A variety of fixes were attempted—changing propellers, changing motors, replacing the autopilot, placing tension straps on the booms to dampen oscillations—but nothing corrected the problem. Flights without the dummy weight were somewhat erratic, but the problem was not as severe. After two days of troubleshooting we decided to fly only the 2×2 NaI detector. Consequently, the pod was packed into its travel case, and a separate Raspberry Pi computer was strapped to the aircraft's landing strut to control the 2×2 NaI detector.

Flights began with a manual takeoff, followed by a short-duration hover, then a climb to the altitude of the first way point, where control was handed off to the mission computer. The pre-loaded mission plans directed the aircraft to fly a raster scan pattern over the radiation area while collecting data. After completing the survey pattern, the pilot-in-charge regained control of the aircraft and landed it. Flights typically lasted about 30 minutes.

Table 3 outlines the flights included in the test execution plan, intended to occur over a four-day period. Unfortunately, troubleshooting the flight instability and deciding to eliminate the Apollo imaging detector consumed two and a half days, leaving a shorter time for actual test flights. With only the 2×2 NaI detector on board, we flew one 15-meter AGL survey on Wednesday in the late afternoon, and then flew six surveys on Thursday The AGL altitudes were 15, 20, 25, 30, 45, and 60 meters.

During a survey flight, data are transmitted to the ground station computers from the Raspberry Pi, and the real-time radiation rates, accumulated spectra, and flight telemetry are displayed on web browser pages. The radiation data are spooled from the detector in list-mode format and are also stored locally on the Raspberry Pi. An array of accumulated spectra is transmitted to the ground station every half second, and the JavaScript routines in the receiving browser compute the differential spectra, smooth the data with exponential moving average filters, and plot strip charts of the radiation rates using several time constants. Typical strip charts are total radiation counts and windowed counts of several isotopes of interest, such as the 662 keV line of ^{137}Cs. Screen shots from flight 1 on April 25 are shown in Figure 14 for radiation readings and in Figure 15 for flight telemetry.

Figure 16 shows the time series of the total radiation rate for the duration of the flight, and a close-up of the data in the vicinity of the largest count rate. The radiation data are plotted with an exponential moving average time filter and a 0.25-second smoothing of the data. The exponential moving average filtering of the data potentially shows greater detail than the fixed 1-second integration intervals normally used. The correlated latitude and longitude data, plotted below the radiation data in Figure 16, are unfiltered. Analysis

Table 3. ADFM detailed flight plan

FLIGHT #	DESCRIPTION	PAYLOAD	ALTITUDE (m)	EST. FLIGHT TIME (MIN)
1	First flight: Shakedown to test basic equipment	No payloads	5	5
2	First flight with payloads: Test comms, functionality	NaI and CZT	5	5
3	First scan flight, 2 m/s, 20 m outside of furthest source location, config 1	NaI and CZT	10	10
4	First CZT imaging flight, hover in place, config 1	CZT	10	20
5	Second scan flight, 2 m/s, 20 m outside of furthest source location, config 1	NaI and CZT	15	10
6	Second CZT imaging flight, hover in place, config 1	CZT	15	20
7	Third scan flight, 2 m/s, 20 m outside of furthest source location, config 1	NaI and CZT	20	10
8	Third CZT imaging flight, hover in place, config 1	CZT	20	20
9	First scan flight, 2 m/s, 20 m outside of furthest source location, config 2	NaI and CZT	10	10
10	First CZT imaging flight, hover in place, config 2	CZT	10	20
11	Second scan flight, 2 m/s, 20 m outside of furthest source location, config 2	NaI and CZT	15	10
12	Second CZT imaging flight, hover in place, config 2	CZT	15	20
13	Third scan flight, 2 m/s, 20 m outside of furthest source location, config 2	NaI and CZT	20	10
14	Third CZT imaging flight, hover in place, config 2	CZT	20	20

of these data can localize the center of the source array and specify its geographical extent. The radiation data shown here, from Flight 1 on April 25, 2019 do not show any distinct undulations from separate discrete sources, but the data merely indicate a smooth distribution that one would expect from a continuous source.

Gamma spectra from the data integrated over the entire flight is shown in Figure 17a and for 5 seconds of data at the time of the highest radiation rate (08:38:25 EDT) are shown in Figure 17b. Lines from ^{137}Cs (662 keV) and ^{60}Co (1170 and 1330 keV) are visible in both spectra, and the spectrum generated from integrating the data over the entire flight shows a small line in the vicinity of 350 keV. This could be the 356 keV line from ^{133}Ba, or it could be the 344 keV line from ^{152}Eu. No other lines from either of these isotopes is visible, so we cannot conclude that either ^{133}Ba or ^{152}Eu was present in the source distribution.

Figure 18 shows a few results from the Laplacian Eigenmap analyses. The technique is a locality-preserving dimensional reduction procedure and an unstructured machine learning algorithm that attempts to classify spectra by means of nearest neighbor features. We hoped that spectra collected during a flyover of a ^{137}Cs source would be distinguishable from those of a ^{60}Co flyover. However, the classifications of these data were simply grouped by instantaneous radiation rates and not by spectral origin.

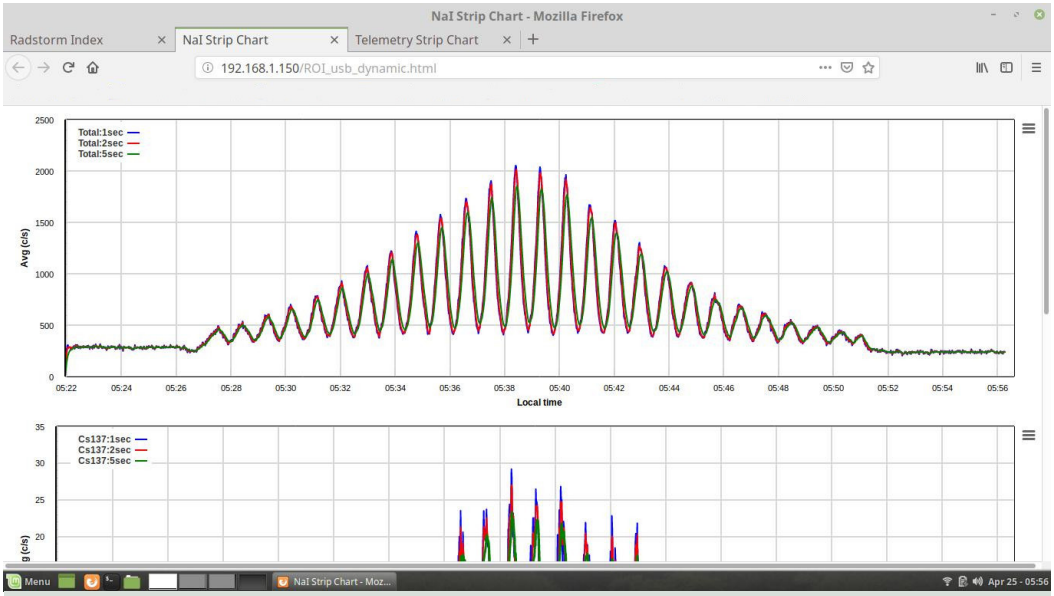

Figure 14. Screen capture of web browser interface plotting real-time radiation data

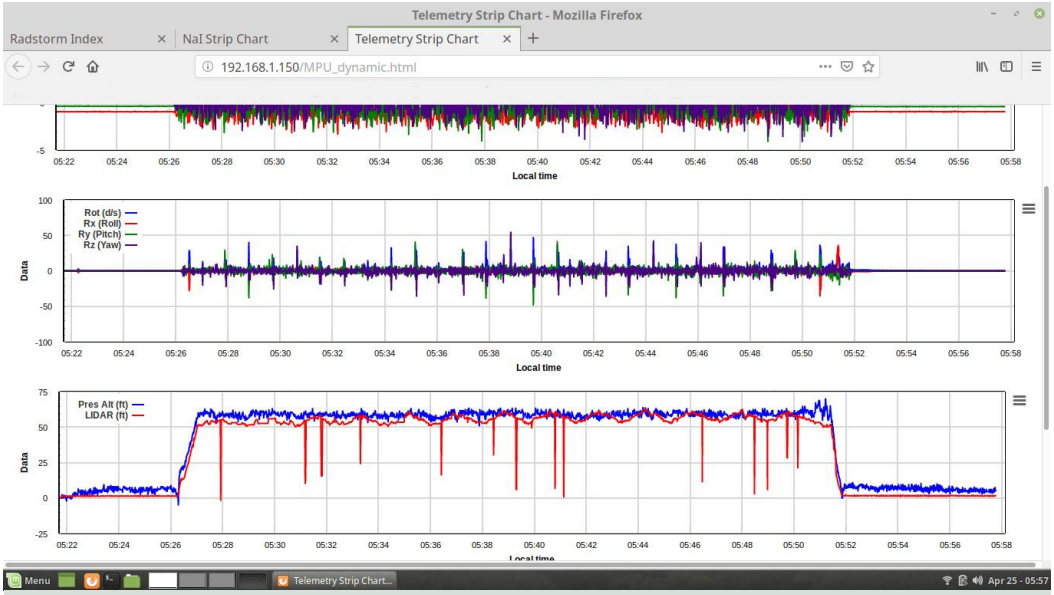

Figure 15. Screen capture of web browser interface plotting real time flight telemetry

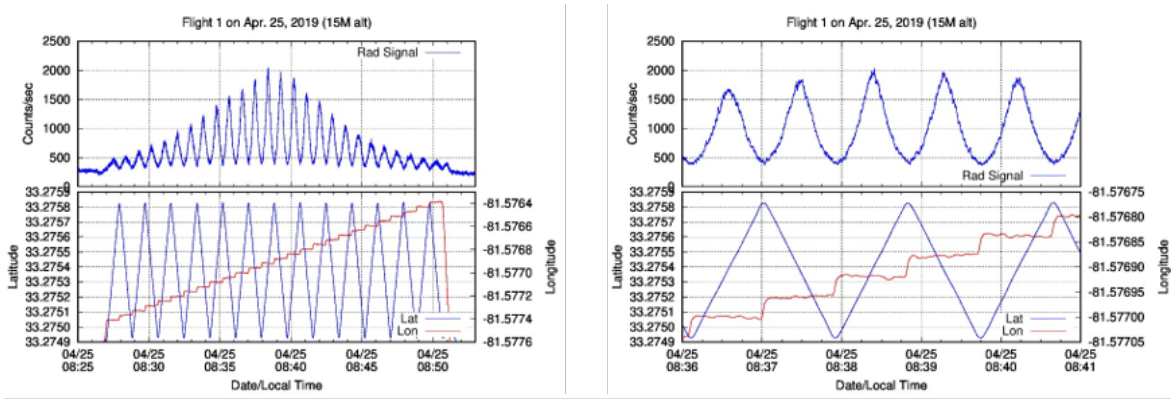

Figure 16. Time series data from the survey flights show smooth behavior of the radiation counts. Exploiting the data can localize the center of the source array and determine its size, but cannot distinguish separate discrete sources.

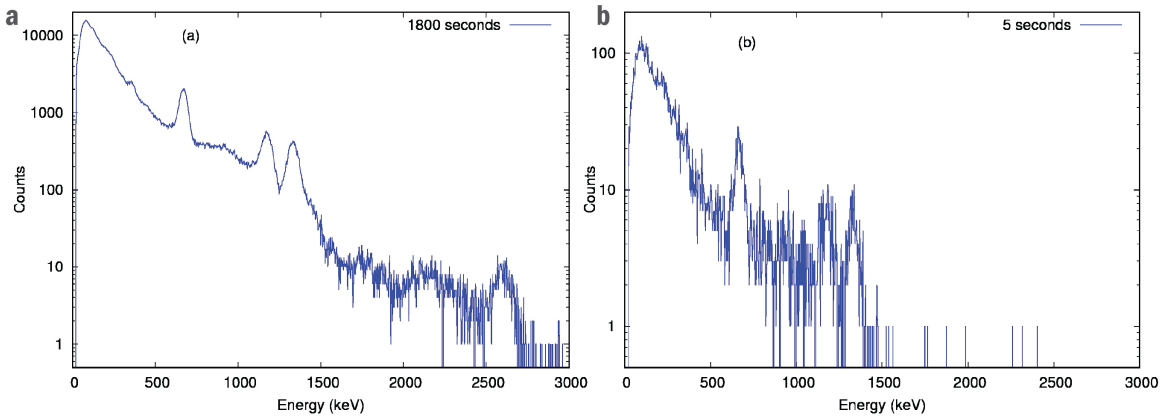

Figure 17. Gamma spectra from flight 1 on April, 25, 2019, showing spectra (a) produced by using data from the entire flight and (b) from 5 seconds of data at the time of the highest radiation rate

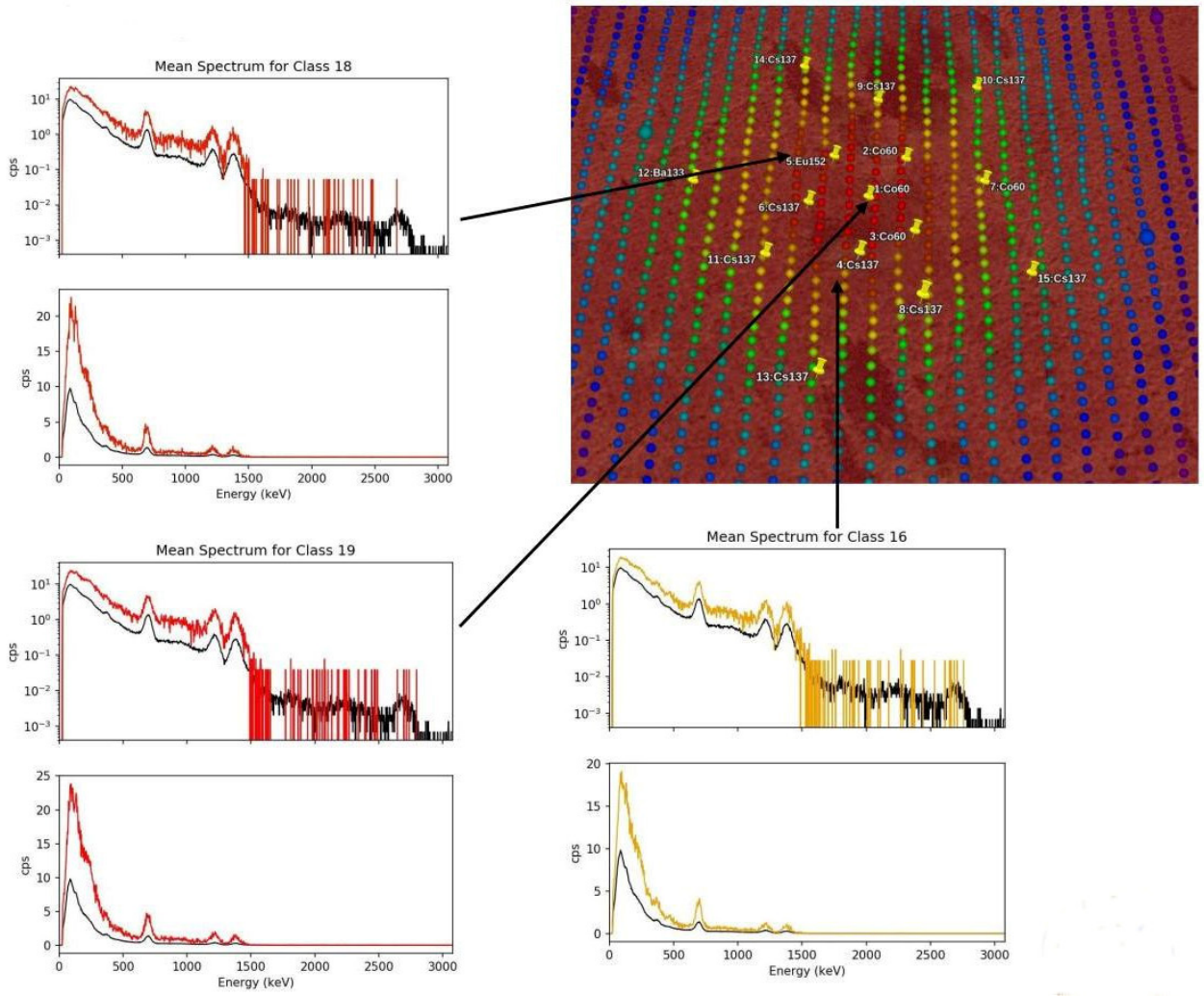

Figure 18. The Laplacian Eigenmapping classifications do not distinguish separate discrete sources. All class spectra contain lines from both ^{60}Co and ^{137}Cs.

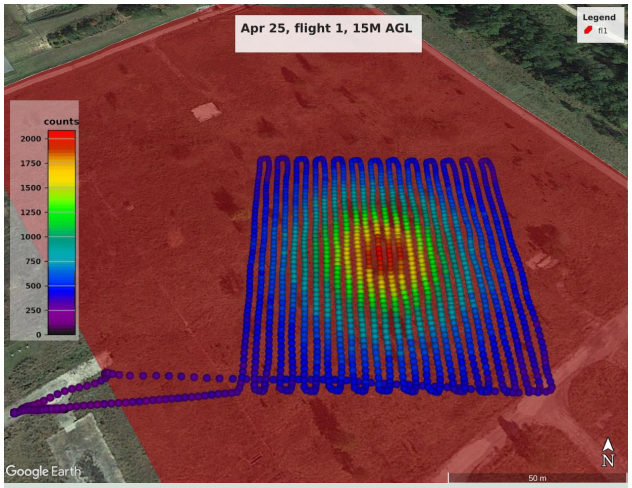

Figure 19. Color-coded breadcrumb trail of measured radiation rates of flight #1

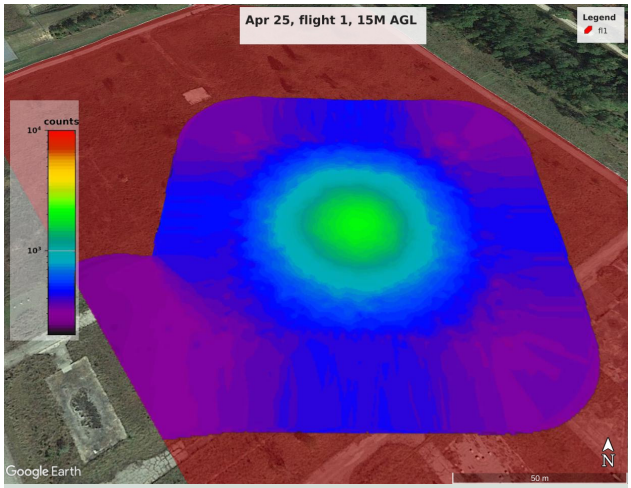

Figure 20. The heat map was produced by Kriging flight #1

In Figure 18 spectra from three classes are shown. Arrows point to locations on the map where the data were collected, and all the radioactive sources are also marked. The spectra are differentiated by the total counts, and differences in ratios of ^{137}Cs to ^{60}Co are not obvious.

The other five flights on April 25, 2019 were at progressively higher altitudes. Our intent was to gauge the degradation of the derived results as the signal dropped closer and closer to the noise floor. At the highest altitude of 60 meters AGL the sources on the ground are still detectable, and the center of the array can still be localized to some extent, but the signal is beginning to be buried by the noise. Extracting a width of the distribution produces error bars nearly as big as the width of the distribution. Also, the 60-meter AGL survey was terminated abruptly because of loss of RTK (Real Time Kinematic) GPS correction, so the scan did not cover the full extent of the source array.

Finally, Figure 19 shows the color-coded breadcrumb trail of instantaneous radiation rate for the flight, and Figure 20 shows a heat map generated by Kriging (i.e., Gaussian interpolation).

Results

Objective 1, proving the reliable the operation of the aircraft, was not fully realized. (Objectives are shown in Table 2.) When trying to lift a heavy payload the aircraft became unstable, and two days of troubleshooting did not resolve the problem. An erratic accelerometer in the Pixhawk autopilot was found to be the cause, but this fault was discovered after the aircraft was returned to Va Tech. Because of this problem, the Apollo detector did not fly during the exercise.

Objective 2 was to prove reliable operation of the detector payloads. This objective was met. Ground checks of both the Apollo and the NaI detectors were good, and the NaI collected data were good from all seven surveys flown.

Objective 3 was to collect data from the surveys using the NaI detector. The performance measure and success criteria were met; however, a classified source map of discrete sources was not realized. Although such a map was our expectation, upon consideration, it is not surprising that it did not result. While the data from the 2×2 NaI detector do clearly define the source center and its extent, the analyses performed thus far do not discern discrete sources; rather, the breadcrumb overlays and heat maps indicate a continuous distribution. Further analyses may produce different results, but that prospect seems unlikely considering the Poisson fluctuations of the data. The raw data are in list-mode format, so different integration times, other than 1-second intervals, can be chosen for an analysis, but longer integration times would smear out the spatial resolution. Because the aircraft was flying at 2 meters/second, intervals longer than about 2 seconds for signal integration would improve counting statistics, but it would also smear sources separated by 8 meters into each other. By contrast, a shorter integration time would preserve geographic fidelity, but Poisson fluctuations would increase and mask any structure in the radiation data spatial curve. Flying at lower altitudes, 10 meters AGL or lower, would likely have produced data showing discrete sources, but the pilot-in-charge was uncomfortable flying an unstable aircraft any lower than 15 meters AGL.

Overall, objective 3 can be considered a near success. The spectra unambiguously show ^{60}Co and ^{137}Cs. There

are hints of ^{133}Ba and ^{152}Eu, but their presence is not statistically justified by the data. The results of the analyses do accurately locate the center of the source distribution and its extent, although the analyses suggest a continuous source distribution of ^{60}Co and ^{137}Cs.

Objective 4 was to collect data using the Apollo detector, but the flight instability of the hexacopter prevented any data collection with the Apollo. Consequently, objective 4 must be considered a failure. Had the detector flown, we are confident from our experience at Huckleberry Hustle that the data would have been good and that individual sources would have been located and identified. It was truly a disappointment to have finished Hyperion Horntail without collecting any data with the Apollo.

For future operations, it would be advisable to have a backup aircraft. Although another hexacopter was available at Va Tech, we left it behind to reduce the amount of equipment we needed to transport. At the exercise we did have an extra 2×2 NaI detector, payload computer, laptop computers, etc., but only one Apollo (because only one exists) and one hexacopter. Also on hand was a 3DR Solo quadcopter to carry the 2×2 NaI detector in the event that the hexacopter would be unable to fly, but the hexacopter was able to fly with the lighter payload.

Figure 21. The USI Sandstorm on the McMillan runway with the detector pod attached to the belly of the fuselage. Todd Bagley (left) and Hovig Yaralian (right) of USI are completing final checks before flight.

JIFX 19-4

The Joint Interagency Field Experimentation (JIFX) campaigns are hosted by the Naval Postgraduate School four times a year at Camp Roberts, which is near Paso Robles, California. JIFX 19-4 occurred during the week of August 4, 2019, and our objectives were to demonstrate a full one-hour grid aerial radiological survey flight with the Sandstorm-T UAS and to learn lessons or technical modifications required to perform a similar survey over the Baneberry crater contamination site at the NNSS later in FY 2020. Flying the initial tests at Camp Roberts would demonstrate our ability to fly beyond visual line of site (BVLOS) in controlled airspace without risk of radioactive contamination of the aircraft.

Figure 21 shows the Sandstorm on the McMillan runway. The pod containing the 3×6 NaI gamma detector is attached to the belly of the fuselage. The pod weighs ten pounds, seven of which are the detector itself. The detector volume is 700 ml, and its gamma energy resolution is 6% at 662 keV. The full-scale energy range is from 30 to 3000 keV. Data are streamed in list mode, meaning that each gamma interaction is recorded with a time stamp and an ADC reading of its energy. The data stream has time fiducials written into it each second, and the clock for the fiducials is the system clock of a Raspberry Pi 3B referenced to a GPS receiver with a 1 pulse per second strobe output. The precision of the clock is better than 1 µs, and the absolute accuracy has been measured to be within 30 µs absolute time of day. The Raspberry Pi in the pod also has a 10DOF telemetry chip interfaced over the I2C bus, and a LIDAR range finder connected over USB. The pod generates datasets of radiation data, GPS coordinates, absolute time of day, accelerations, rotations, magnetometer readings, temperature, atmospheric pressure, pressure altitude, and LIDAR distance above ground. The pod is self-contained, operates independently of the aircraft, and has its own power supply and communication capabilities. For the JIFX experiment, the communications to the ground station were over 915 MHz using a pair of RFD900x radios, however in previous exercises we have used 2.4 GHz Wi-Fi, and 4G LTE cellular data links.

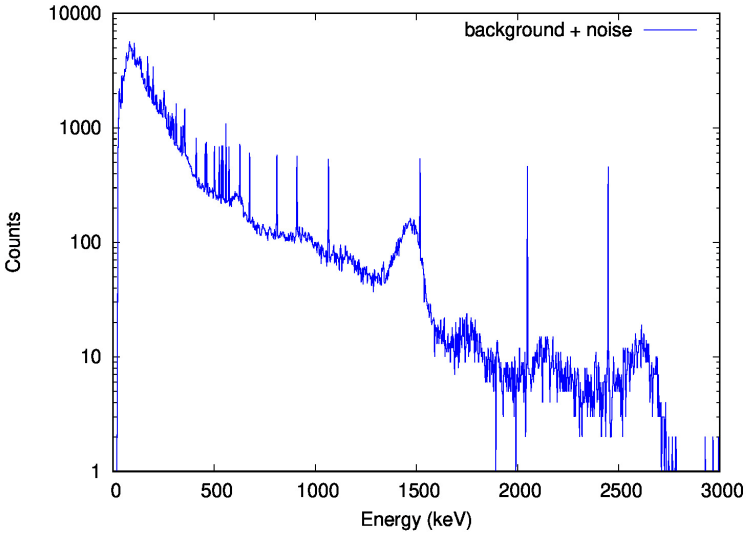

Figure 22. Gamma spectra show the usual natural background emissions of ^{214}Bi at 609 keV, ^{40}K at 1461 keV, and ^{208}Tl at 2614 keV. The sharp spikes are noise caused by the 915 MHz Microhard radio of the Piccolo autopilot.

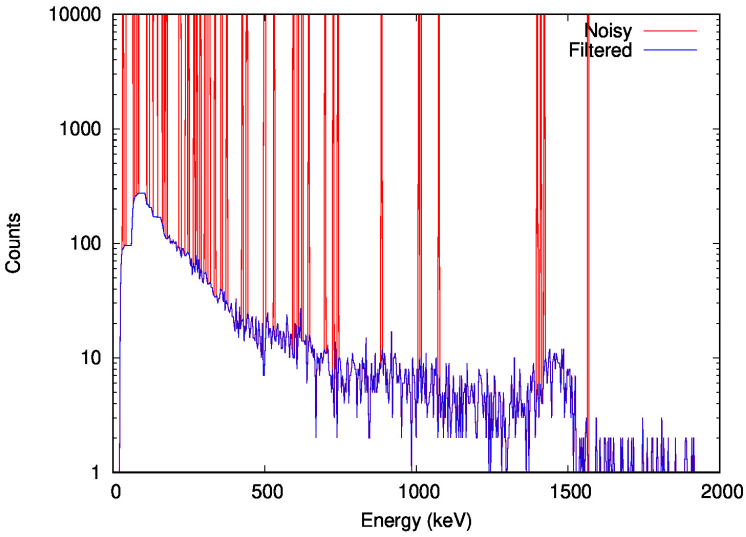

Figure 23. The noise spikes occurring during flight have been digitally filtered to show the background radiation

On Tuesday, August 6, 2019, we launched at 9:28 a.m. and conducted a 61-minute flight. The aeronautical flight was a success—a full survey grid was flown and much of the flight was BVLOS. Unfortunately, as soon as the Piccolo autopilot system was brought online, noise was introduced on the radiological data transmission channel, and the radiation data were lost. Afterward, different antennae positions were tried, but none were effective. However, transitioning from spread spectrum to one-channel RF transmission of the radiation data appeared to correct the issue, so we decided to conduct another flight on Wednesday.

On Wednesday, August 7, 2019, we launched at 9:17 a.m. We successfully flew a coarse lawn-mower pattern for 29 minutes, much of it BVLOS. But again, when the Piccolo autopilot system was initiated noise infiltrated the radiological data transmission channel; however, this time, we recovered some of the data. While landing, the Sandstorm hit an unpatched crack in the runway and exited the runway, damaging its propeller. With most objectives completed, we stopped operations at JIFX 19-4.

Figures 22 and 23 show gamma spectra containing noise measured by the 3×3 NaI detector in the pod. The noise appears as sharp pikes in the data, and we traced its origin to the Piccolo's 915 MHz Microhard radio. The other 915 MHz RFD900x radio did not appear to cause noise issues, but communications over the RFD900x experienced substantial dropout issues once the Microhard radio was powered on. We attempted to rearrange antennas, to shield the pod, and to reprogram the broadcast spectrum of the two radios, but to no avail. The Piccolo autopilot system automatically programs the Microhard radio and leaves very few options to the user. We attempted to use only one half of the 902 to 928 MHz band, putting the radios into separate non-overlapping frequency bands (902–915 MHz and 915–928 MHz), but the Piccolo overrode our attempts to reconfigure the Microhard radio. The RFD900x was reprogrammed without issue, and it was ultimately configured to broadcast on a single channel at 928 MHz, but the RFD900x appeared not to be causing the problem.

Even after adjustments, we still noted a sporadic noise problem, but we decided to fly the mission. Figure 24 shows the flight track flown on Tuesday, August 6, 2019. The track combined aerial serpentine and lawn mower patterns into a single flight, because there was neither radioactive contamination nor gamma sources fielded at Camp Roberts. Normally, the two patterns would be flown separately. First the serpentine pattern is done as an initial search. The lawn mower

pattern then focuses on the radiation hot spot identified by the serpentine search, collecting data for a heat map of the radiation on the ground. Over 61 minutes the Sandstorm flew about 2.3 miles from the ground station, completing a true BVLOS mission. The communications link from the detector pod dropped shortly after takeoff, but the detector is configured to collect data and store it locally, irrespective of the communications link.

After the flight we discovered that the gamma detector had locked up early in the flight, and that no gamma data had been collected. This was an unusual occurrence, since a hard lock-up of the detector is a very rare event in our experience. We attempted additional fixes (e.g., adding shielding, relocating the antenna) and planned to fly again early Wednesday morning.

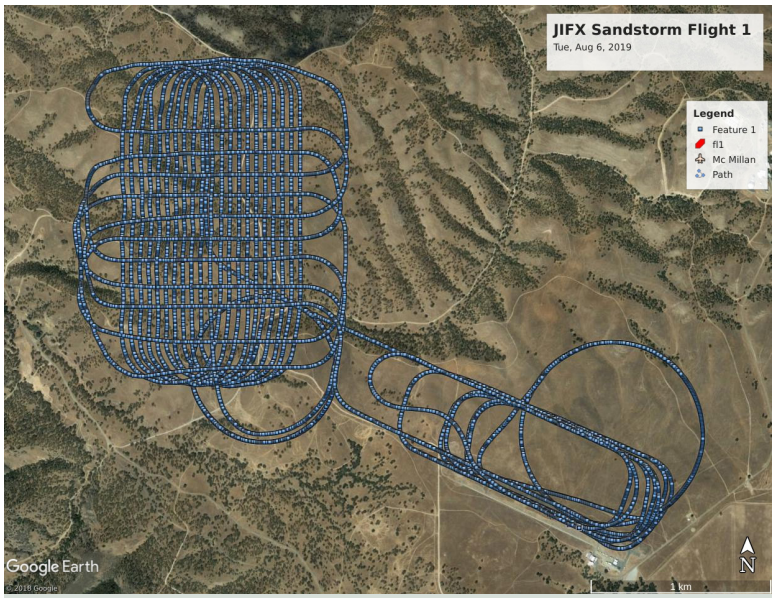

Figure 24. The first Sandstorm flight lasted 61 minutes, and it consisted of a serpentine search pattern followed by a lawn mower mapping pattern

The second Sandstorm JIFX 19-4 flight, a coarse lawn mower pattern (Figure 25), lasted 29 minutes. Shortly after takeoff the pod's communications link dropped again, and the data stream was plagued by noise. The solution to the problem will undoubtedly involve replacing the Piccolo's Microhard radio with an RFD900x and adding additional RF shielding to the pod.

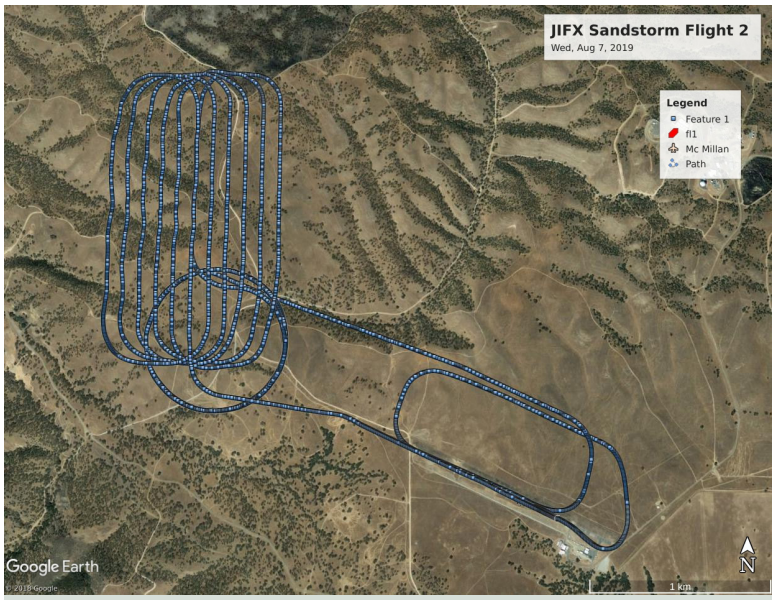

Figure 25. The second Sandstorm flight lasted 29 minutes, and it was a coarse lawn mower pattern

Although we patched the runway asphalt significantly the week prior to JIFX, the condition of the McMillan runway was marginal. During its second flight landing, the Sandstorm ran off the side of the runway; apparently one of the landing gears hit a crack that we had not patched. Fortunately, the Sandstorm had nearly stopped at that point, so the aircraft and detector pod were mostly unscathed. However, the propeller was damaged, so we decided that any further flying would be too risky. Consequently, we left Camp Roberts on Wednesday afternoon, but Paul Guss remained to attend the debriefing.

A contributing factor to the difficulties we had with the runway is the inadequate airspace ahead of the top of the runway. To make full use of the runway section that we had patched a proper approach would have necessitated flying outside of sector 1F. The air boss informed us that breaking the airspace was strictly prohibited, even if it meant that a third of the runway would be consumed by the final approach glide angle, and that we would fly over most of the runway section that we had patched. This limitation of the airspace boundary would not have been a problem if the surface condition of the entire runway had been adequate. Nevertheless, it is a curious situation for an airspace boundary to prohibit full use of the runway for fixed-wing aircraft.

Figure 26. The Harris H6 hexacopter has a gasoline-powered generator to maintain battery charge for two hours of flight. It is shown here carrying the STL 3×6 NaI radiation detection pod.

JIFX 20-1

The JIFX 20-1 event occurred during the week of November 4, 2019. Our objective for the event was demonstration of BVLOS radiation survey patterns conducted by a long duration heavy-lift hexacopter while utilizing a separate aircraft acting as a communications relay. The survey aircraft was a Harris model H6 hybrid hexacopter, and the original communications relay aircraft was an Albatross fixed-wing drone. Figure 26 shows the Harris H6 with the STL 3×6 NaI radiation detection pod attached beneath the chassis next to the two-stroke gasoline engine–powered generator. The generator charges two 6S LiPo batteries during flight. In the event of a generator loss of power, the batteries can support about 10 minutes of flight time to execute an emergency landing.

The first test flight of the Harris H6 hexacopter was at 3 p.m. on Monday afternoon, November 4, 2019, along the McMillan runway with a 10-pound dead weight. During this flight the Albatross remained on the ground, but did act as the communications relay. This flight was a success. Afterward, the dead weight was replaced by the 3×6 NaI detector pod, and the multi-point communications radios were tested in the hangar. No further flight windows were available on Monday. On Tuesday we executed no flights, because another group at JIFX accidentally violated restricted airspace, causing the entirety of Camp Roberts to go into security lock-down. We flew three flights on Wednesday, November 6, 2019.

The first flight was launched at 9:26 a.m., and it lasted 3 minutes. It was a short flight along the runway, which was successful.

For the second flight we attempted to launch the Albatross, but during roll-out it hit a crack in the pavement and ran off the runway. Figure 27 shows the Albatross and the Harris H6 on the McMillan runway. The runway incident damaged the Albatross

Figure 27. At the left is the Albatross fixed-wing sUAS, which was intended to be a radio communications relay. On the right is the Harris H6 hexacopter that flew the survey pattern.

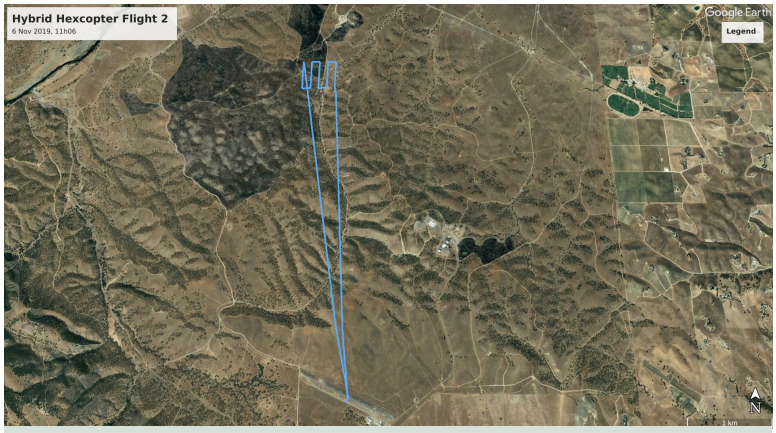

Figure 28. The Harris H6 hexacopter flew a coarse survey grid pattern at a distance of 2.9 miles from the launch point. The CACTF site can be seen just slightly north of the grid.

propeller, and because a replacement was not available, the Albatross was grounded for the rest of the event. During the second flight the grounded Albatross served as the communications relay. The Harris H6 was launched on its mission at 11:06 a.m.; at ~1 mile out, the communications dropped for both aircraft control and pod data. The Pixhawk autopilot, however, had been configured to continue the mission in the event of a communications failure, so the mission completed successfully with full datasets. Figure 28 shows the flight path as constructed from GPS data collected from the GPS receiver in the 3×6 NaI detector pod.

For the third flight, we considered that having the relay aircraft sitting on the ground next to the ground control station was not ideal for a BVLOS mission, so the backup Harris H6 hexacopter was configured to be the communications relay aircraft. It was flown to an altitude of ~1000 ft AGL, configured to fly a box pattern ~1 mile from the ground station. The hexacopter carrying the pod was programmed with a flight plan of an expanded lawn mower search grid at the same location just south of the Combined Arms Collective Training Facility (CACTIF) site. The flight lasted 36 minutes. Although communications dropped again ~1 mile out, as before, the Pixhawk autopilot had been configured to continue the mission in the event of a communications loss. Full telemetry and radiation data were collected, but no radiation sources were on site, so the data consist entirely of background radiation readings.

Figure 28 shows the flight path recorded by the GPS receiver in the detector pod. Figure 29 shows both hexacopters in the air. The one in the foreground is

Figure 29. After the incident that disabled the Albatross, a second Harris H6, seen in the distance, was used as the communications relay. The hexacopter carrying the 3×6 NaI detector pod is in the left foreground.

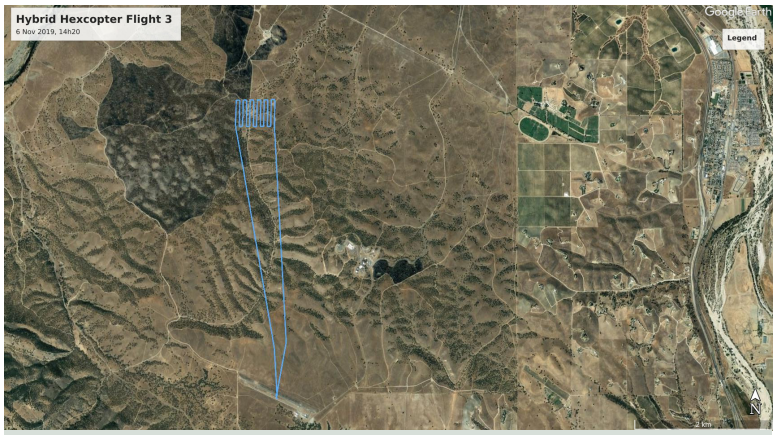

Figure 30. A denser survey grid was flown over the same location as the coarse grid. Communications were lost during both flights, but the autopilot was programmed to fly complete mission without communications.

the copter that flew the detector. Figure 30 shows the hexacopter's flight path measured by the pod's GPS receiver. Figure 31 shows pressure altitude and LIDAR altitude ranging data recorded by the pod.

During the third JIFX 20-1 flight, the altitude above ground of the hexacopter was beyond the range of the LIDAR. Those regions are obvious in the plot, but at the beginning and end of the flight the LIDAR data show terrain contours as the flight proceeded out and back again. Figure 32 shows the radiation rate measured by the 3×6 NaI gamma detector. The signal is due to the natural radiation background, and the variations seen in the plot are due primarily to different altitude positions of the detector. Because of atmospheric scattering and attenuation due to Compton scattering, the radiation level drops with increasing altitude.

The primary JIFX 20-1 objective to fly BVLOS with full data collection was satisfied by these two flights. The problem with radio communications could not be corrected in the field, and we concluded JIFX 20-1 operations at Camp Roberts on Wednesday afternoon.

Conclusion

We have made considerable progress in our attempts to demonstrate autonomous beyond visual line of sight survey flights of UAS carrying radiation and chemical detectors. The Sandstorm fixed-wing and the Harris H6 rotary platforms are both suitable for two-hour-long heavy-lift missions. To date, both aircraft have carried the ten-pound STL 3×6 NaI radiation detection pod to distances beyond two miles from the launch point, flying fully autonomous missions of lawn mower search patterns. Issues with real-time communications for flight control and data feeds are still dogging us, however. The various radios that we have used have not successfully operated at the distances specified by the manufacturers, and we are continuing to test antenna configurations. Cellular data feeds do work when coverage is available, but our flight tests thus far have been in areas of poor cellular coverage. When

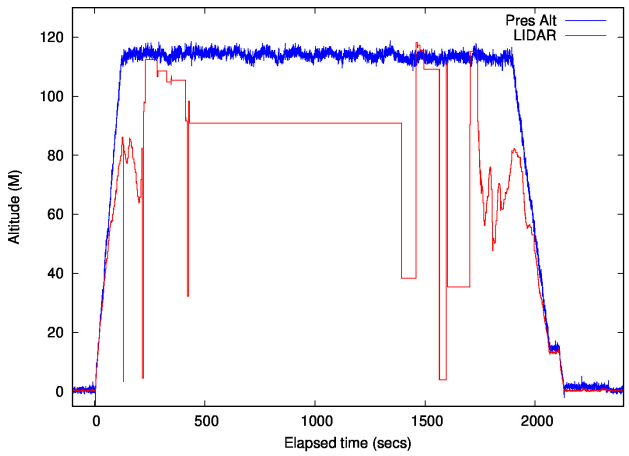

Figure 31. Pressure altitude is insensitive to terrain changes that LIDAR ranging can detect. However, for part of this dataset the LIDAR was operating at an altitude beyond its sensitivity limit.

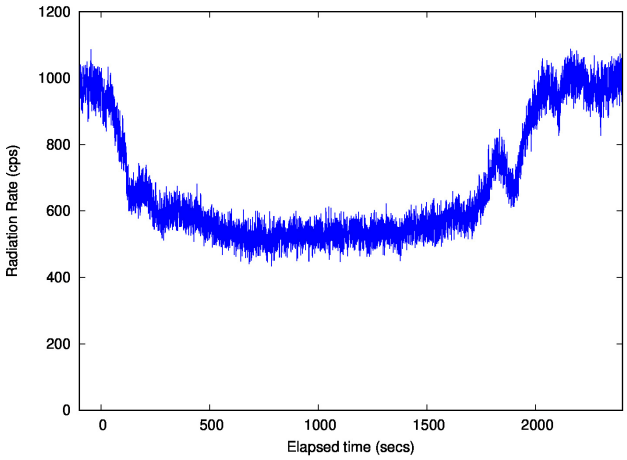

Figure 32. The measured radiation rate is from the natural radioactive background. The variation is due primarily to the distance above ground and atmospheric attenuation from Compton scattering.

the ground station can connect to the relay virtual machine on the Amazon cloud, real-time monitoring of the flight and data feeds is possible over the internet.

The demonstrated sUAS capabilities should allow for enhanced AMS-style missions by offering the capability to provide high-density sampling, sample locations that are difficult to access, and flying in conditions that are too hazardous for manned aircraft. Realistically, the systems have been deployed in relevant environments, which is nominally TRL 6. Over the past year we have presented our work at the Military Sensing Symposium, at the VIP day at Savannah River National Laboratory, and at the EMI Sig annual meeting in Knoxville. We have also submitted several white papers to various federal funding agencies.

Acknowledgments

We would like to thank Drew Morgan, John Peterson, and Anthony Wagner for piloting and ground control station assistance in the Hyperion Horntail exercise. We wish to thank Hovig Yalarian, Todd Bagley, and Allan Horzewski for assistance at Camp Roberts during the JIFX events.

References

Belkin, M., P. Niyogi. 2003. "Laplacian Eigenmaps for dimensionality reduction and data reduction," *Neural Computation* **15**: 1373–1396.

Peterson, J., W. Li, B. Cesar-Tondreau, J. Bird, K. Kochersberger, W. Czaja, M. McLean. 2019. "Experiments in unmanned aerial vehicle / unmanned ground vehicle radiation search," *J. Field Robotics* **36**: 818–825.

Trainham, R., P. Guss, M. Manard, L. McLean, W. Kaye, K. Kochersberger. 2019. "Drone Video Platform – Collision Avoidance, Situational Awareness, and Communications." In *FY 2018 Site-Directed Research and Development Annual Report*, 17–37. Las Vegas, Nevada: Mission Support and Test Services, LLC.

This page left blank intentionally.